

A Statistical Comparison of Cluster Mass Estimates from Optical/X-ray Observations and Gravitational Lensing

Xiang-Ping Wu

Beijing Astronomical Observatory, Chinese Academy of Sciences, Beijing 100080, China

and

Li-Zhi Fang

Department of Physics, University of Arizona, Tucson, AZ 85721

Received 21 October 1996; accepted 24 January 1997

ABSTRACT

We present a statistical comparison of three different estimates of cluster mass, namely, the dynamical masses obtained from the velocity dispersion of optical galaxies, the X-ray masses measured from the temperature of X-ray emitting gas under the assumption of isothermal hydrostatic equilibrium, and the gravitational lensing masses derived from the strong/weak distortions of background galaxy images. Using a sample of 29 lensing clusters available in literature, we have shown that the dynamical masses are in agreement with the gravitational lensing masses, while the X-ray method has systematically underestimated cluster masses by a factor 2-3 as compared with the others. These results imply that galaxies indeed trace the gravitational potential of their clusters, and there is no bias between the velocities of the dark matter particles and the galaxies in clusters. The X-ray cluster mass discrepancy is probably from the simplification in the models for the X-ray gas distribution and dynamical evolution.

Subject headings: cosmology: theory — galaxies: clusters: general — gravitational lensing

1. Introduction

Clusters of galaxies are the largest coherent and gravitationally bounded objects in the universe. The precise determination of their gravitational masses is crucial for our understanding of formation and evolution of cosmic structures, for mapping of matter distribution on large-scales and also for measurement of the present mean mass density of the universe (Ω_0). Historically, cluster masses are derived from the dynamical analysis of the observed velocity dispersion of cluster galaxies based on the virial theorem, which results in the so-called virial cluster masses M_v . With the development of the X-ray astronomical techniques clusters can be selected from the X-ray emission of the hot diffuse intracluster gas, giving rise to the X-ray cluster masses M_x when combined with the assumption of hydrostatic equilibrium. Over the past decade the detection of the gravitationally distorted images of faint distant galaxies behind some clusters of galaxies provides another independent mass estimate: the gravitational cluster masses M_{lens} . In particular, M_{lens} are obtained regardless of the cluster matter state and components. These three methods should be incorporate, and comparisons of their results would yield a very useful clue regarding the dynamical evolution of clusters and a test for the accuracy of cluster mass determinations.

The early studies based on a few selected clusters in which both lensing and optical and/or X-ray data are available claimed a cluster mass discrepancy by a factor of typically $2 \sim 3$ among the three methods (Wu, 1994; Fahlman et al. 1994; Miralda-Escudé & Loeb 1995), while a consistency between dynamical masses and gravitational lensing derived ones has been also reported in some cases, e.g. PKS0745-191 (Allen, Fabian & Kneib 1996). We have recently carried out a statistical comparison of the overall cluster radial matter distributions determined from X-ray observation and gravitational lensing and concluded that the X-ray analysis may have systematically underestimated cluster masses at least in

the central regions (Wu & Fang 1996; hereafter Paper I).

From the theoretical point of view, the above three methods have to give the same cluster masses if clusters are dynamically relaxed. This probably accounts for the result in clusters like PKS0745-191 which appear to be regular in optical/X-ray morphologies. Though one may attribute the reported mass discrepancy to the nonthermal pressure (Loeb & Mao 1994; Ensslin et al. 1997) or the projection effect (Miralda-Escudé & Babul 1995; Cen 1996), it is most likely that the problem is relevant to the cluster matter distribution and dynamical evolution. Indeed, both optical and X-ray observations have revealed the presence of substructures in most of clusters, implying that clusters may be still in the era of formation. In particular, the recent spatially-resolved measurements of gas temperature in some clusters illustrate the complex two-dimensional patterns including the asymmetric variations and the significant decline with radius (e.g. Henriksen & White 1996; Henriksen & Markevitch 1996; Markevitch 1996), which are the strong indicators of the effect of substructure merging. For those clusters, we are unable to apply the equation of hydrostatic equilibrium to the X-ray emitting gas. Therefore, it is naturally expected that the X-ray cluster mass obtained under the assumption of a hydrostatic equilibrium is in principle not representative of the true cluster mass, and thereby should be different from the gravitational lensing derived mass and/or even the virial mass. This scenario is supported by the recent numerical study of X-ray and lensing properties of clusters of galaxies from the standard CDM simulations by Bartelmann & Steinmetz (1996). They found that the cluster masses can be biased low if the traditional β model is adopted for the intracluster gas, which is especially true when clusters exhibit pronounced substructures, while the strong lensing preferentially selects the clusters that are dynamically more active than the average.

Alternatively, it should be noticed that M_v derived from the virial theorem and M_x

derived from the hydrostatic equilibrium have very different physical implications. M_v is related to the galaxy velocity dispersion and galaxy number density. Comparison of M_v and M_{lens} would set constraints on the bias parameter between the velocities of the galaxies and of the dark matter and test whether optical galaxies trace the gravitational potential of the cluster. On the other hand, M_x depends on the temperature variation and the density profile of the hot diffuse gas, which may suffer from the influence of the possible existence of the turbulence and magnetic field. As a result, comparison of M_x and M_v may allow one to determine how significant the nonthermal pressure contributes to the computation of M_x because galaxies are unaffected by the nonthermal pressure in clusters. Furthermore, the comparison of the three cluster estimates may help to solve the puzzle of the baryonic matter excess in clusters if clusters provide a fair sample of the universal baryon fraction (see Paper I for summary). Recall that the baryon fractions in clusters are computed using the dynamical masses M_x and/or M_v , which may have large uncertainties if most of clusters are still in the process of violent merging. As a whole, galaxies and gas particles have probably experienced very different evolutions in the formation of clusters and then exhibit different dynamical states and density distributions in clusters today.

Numerous lensing and optical/X-ray observations of clusters have now made it timely and possible to carry out these comparisons. Unlike Paper I that chose X-ray and lensing data separately from literature, we now work with the lensing clusters only, in which the strongly and/or weakly distorted images of background galaxies have been observed. While this paper was in the refereeing stage, we received a preprint by Smail et al. (1997) who made a similar but sophisticated investigation for 11 distant clusters observed with *HST*. Throughout this paper we adopt a matter-dominated flat cosmological model of $\Omega_0 = 1$ and a Hubble constant of $H_0 = 50 \text{ km s}^{-1} \text{ Mpc}$.

2. Cluster sample and mass estimates

Strongly/weakly distorted images of background galaxies have been so far detected in ~ 40 clusters of galaxies (Fort & Mellier 1994; Wu 1996; Van Waerbeke & Mellier 1996). For our purpose we only select those lensing clusters whose X-ray luminosity(L_x)/temperature(T) and/or optical galaxy velocity dispersion (σ) are available in literature. This results in a non-exhaustive list of lensing cluster sample (Table 1) containing 29 clusters and 39 measurements.

EDITOR: PLACE TABLE 1 HERE.

Temperature of the hot diffuse gas is the most important parameter for the X-ray cluster mass determination. Unfortunately, only few clusters in Table 1 have the measured temperature: A370 ($T = 8.8 \pm 0.8$ keV), A1689 ($T = 10.1^{+5.4}_{-2.8}$ keV), A2163 ($T = 13.9$ keV), A2218 ($T = 6.7$ keV), MS0451($T = 10.4 \pm 1.2$ keV) and PKS0745 ($T = 8.6^{+1.1}_{-0.9}$ keV). This arises from the difficulty of the X-ray spectroscopic observations. Nonetheless, a correlation between cluster temperature and bolometric X-ray luminosity $L_{x,bolo}$ has been well established (e.g. Edge & Stewart 1991; Fabian et al. 1994): $L_{x,bolo} = 10^{43.06 \pm 0.08} T^{2.68 \pm 0.10}$ while L_x in unit of erg s^{-1} can be relatively easily obtained. Such a relationship thus enables us to translate L_x into T . Assuming a mechanism of free-free bremsstrahlung for the gas-emission and adopting an approximate Gaunt factor given by Mewe et al. (1986), we have computed the cluster temperature T for each cluster in Table 1. Note that the error bars in the resulting T account for both the uncertainties of the L_x measurement and of the L_x - T relation. It is seen that the agreement between the measured temperature and the estimated one is fairly good for the above six clusters.

Cluster optical and X-ray morphologies reflect their dynamical state at different evolutionary stages, which turn to be quite varied observationally. Apparently, a well-

relaxed system would appear to be regular. MS0440 and PKS0745 in Table 1 might be two good examples of this kind. On the other hand, clusters that are currently forming may have very irregular morphologies. Substructures in optical/X-ray images are the most common feature in those clusters and on-going collisions of the substructures are the most convincing evidence for interaction. Another indicator for the cluster non-hydrostatic process is the complex temperature patterns observed recently from a number of spatially resolved measurements of the gas temperature. All these sorts of clusters are marked by “I” in Table 1. Moreover, we utilize “E” to denote the rest clusters in which substructures do not clearly present but their X-ray/optical maps look more or less like ellipses in shape.

Fitting the azimuthally averaged X-ray surface brightness profile by the usual β model and assuming a hydrostatic equilibrium for the X-ray emitting gas, we can obtain the projected X-ray cluster mass m_x within cluster radius r through (Wu 1994)

$$m_x = 1.13 \times 10^{14} M_{\odot} \beta_{fit} \left(\frac{r_{xc}}{\text{Mpc}} \right) \left(\frac{kT}{\text{keV}} \right) \tilde{m}(r), \quad (1)$$

where

$$\tilde{m}(r) = \frac{(R/r_{xc})^3}{(R/r_{xc})^2 + 1} - \int_{r/r_{xc}}^{R/r_{xc}} x \sqrt{x^2 - (r/r_{xc})^2} \frac{3 + x^2}{(1 + x^2)^2} dx$$

and r_{xc} and R are the core radius in β model and the cluster physical radius, respectively. A straightforward computation shows that \tilde{m} depends very weakly on R and we will thus take a value of $R = 3$ Mpc in the following calculation.

We now give another way to estimate the cluster mass. We model the cluster matter distribution by an isothermal sphere which is characterize by a core radius r_{dc} and the optical galaxy velocity dispersion σ . We use the term “virial” or “dynamical” cluster mass to denote the mass given by the optical galaxy velocity dispersion, though this differs from the usual virial analysis which utilizes the galaxy number density in cluster rather than the dark matter profile. Our attempt here is to examine whether σ can provide a good mass estimate when compared with gravitational lensing method. Yet, the radial galaxy

distribution in cluster is not well constrained. Recall that the traditional King model has been questioned (Bahcall & Lubin 1994). For a softened isothermal sphere, the projected “virial” mass within a radius of r is simply

$$m_v = \frac{\pi\sigma^2}{G} r \left(\sqrt{1 + \frac{r_{dc}^2}{r^2}} - \frac{r_{dc}}{r} \right). \quad (2)$$

Finally, with gravitational lensing method one is able to determine the projected gravitational cluster mass within the arc position r_{arc} or the distance r from the cluster center on the cluster plane:

$$m_{lens} = \begin{cases} \pi r_{arc}^2 \Sigma_{crit}, & \text{for arc/arclet;} \\ \pi r^2 \zeta(r) \Sigma_{crit}, & \text{for weak lensing,} \end{cases} \quad (3)$$

where $\Sigma_{crit} = (c^2/4\pi G)(D_s/D_d D_{ds})$ is the critical surface mass density with D_d , D_s and D_{ds} being the angular diameter distances to the cluster, to the background galaxy and from the cluster to the galaxy, respectively, and $\zeta(r)$ measures the statistics of the shear field γ of background galaxy images induced by the cluster (Fahlman et al. 1994). Note that in eq.(3) arclike images have been presumed to trace the Einstein radius of the cluster so that the alignment parameter is approximately taken to be zero. Furthermore, we need to make two remarks: (1) Redshift data are still not available for nearly half of the arcs listed in Table 1, for which we have assumed a redshift of $z_s = 0.8$. This leads to the decrease of mass estimate m_{lens} by a factor of 1.4 for a typical arc-cluster at $z_d = 0.3$ if the background galaxy is set to be $z_s = 2$. (2) Weaking lensing analysis provides only a low bound on m_{lens} .

The resulting three mass estimates have been given in Table 1. Uncertainties in most of the m_{lens} results and some of the m_v results are hard to evaluate at present. Alternatively, in the computation of m_x we adopt a mean core radius of $r_{xc} = 0.25$ Mpc but allow r_{xc} to vary from 0.1 Mpc to 0.5 Mpc. So, the error bars in the final result of m_x include both the uncertainties in T and the ones in r_{xc} . Moreover, all the results of m_x in Table 1 correspond

to $\beta_{fit} = 1$ while the observationally fitted value is around $\beta_{fit} \approx 0.67$ (e.g. Jones & Forman 1984). For the dynamical cluster mass m_v given by the optical galaxy velocity dispersion, we have assumed $r_{dc} = 0$.

3. Results and discussion

Comparisons of cluster mass estimates from X-ray gas hydrostatic equilibrium, dynamical analysis and gravitational lensing are shown in Figure 1(a) and (b) using the data of Table 1. An immediate conclusion is that m_{lens} agrees essentially with m_v while a systematic excess of m_{lens} with respect to m_x is detected. This can be clearly demonstrated by the following best-fit relation to the data:

$$m_{lens} = (1.42 \pm 0.99)m_v = (2.23 \pm 1.15)\beta_{fit}^{-1}m_x, \quad (4)$$

in which the uncertainties are the 1σ errorbars. Meanwhile, Fig.1(a) and (b) also illustrate the influence of cluster morphologies on the relations between m_{lens} and m_v and between m_{lens} and m_x , respectively. Apparently, it is very unlikely that cluster morphologies can lead to a remarkable difference in the results.

EDITOR: PLACE FIGURE 1 HERE.

In Fig.2(a) and (b) we display the variations of m_{lens} , m_v and m_x with the cluster radius. Basically, Fig.2(b) provides a result similar to the one of Paper I, i.e., there is a systematic discrepancy between m_x and m_{lens} inside the cluster core radius, and the projected gravitational cluster mass obtained with lensing method follows a simple power-law of $\sim r^{1.3}$. Again, in contrast to m_x , m_v agrees statistically with m_{lens} over all the scales.

EDITOR: PLACE FIGURE 2 HERE.

Additionally, we have computed the β parameter characterizing the specific energies of the galaxies and the gas in clusters, $\beta_{spec} \equiv \sigma^2/(kT/\mu m_p)$ where $\mu m_p = 0.59$ is the mean particle mass. Our best-fit value with the 18 data points (both T and σ are available) in Table 1 reads $\beta_{spec} = 1.29 \pm 0.71$, while β_{spec} reduces to 1.17 ± 0.50 if AC114 is excluded. The best-fit relation between the galaxy velocity dispersion and the gas temperature is

$$(\sigma/\text{km s}^{-1}) = 10^{2.64 \pm 0.11} (T/\text{keV})^{0.51 \pm 0.13}. \quad (5)$$

It appears that our best-fit average β_{spec} and σ – T relation are consistent with the previous work [see Girardi et al. (1996) for summary]. Based on such a good fitness of eq.(5) alone, one might conclude that the galaxies and the gas are in hydrostatic equilibrium with the same cluster potential, as was claimed by Lubin & Bahcall (1993). However, our result of eq.(4) raises a new question of how one could reconcile the discrepancy between m_{lens} (or m_v) and m_x with the good correlation between σ and T .

Alternatively, it turns out from Fig.1(a) that a zero core radius $r_{dc} = 0$ for the cluster mass profile provides a good fit to the lensing data. The best-fit core radius r_{dc} by requiring $m_v = m_{lens}$ is $r_{dc} = -0.09 \pm 0.24$ Mpc, indicative of rather a compact dark matter distribution in clusters. This result is compatible with the early studies of giant arcs and statistical lensing of arcs/arclets which report a small core radius (< 0.1 Mpc) for the dark matter profile of the arc clusters (e.g. Hammer 1991; Wu & Hammer 1993; Grossman & Saha 1994).

While there is a significant evolution of X-ray luminosity clusters with redshift (Edge et al. 1990; Gioia et al. 1990; Henry et al. 1992), the deficit of the X-ray cluster mass may be relevant to the cluster evolution. Recall that the local L_x – T relation established at low redshift $z < 0.1$ was employed to estimate the cluster temperature, whereas most of the

clusters in Table 1 are actually located at intermediate redshift $z \sim 0.2\text{--}0.5$. Therefore, it would be useful to examine the dependence of the ratio of m_{lens} to m_x on the cluster redshift. Our best-fit relation is

$$\frac{m_{lens}}{m_x} = 10^{0.09 \pm 0.10} (1+z)^{1.7 \pm 0.9} \quad (6)$$

Namely, the cluster mass discrepancy between the X-ray analysis and the gravitational lensing method is indeed related to the evolutionary history of clusters. Since m_x is proportional to T according to eq.(1), the cluster temperature has a similar variation with redshift. This yields a temperature ratio of $1.5^{+0.4}_{-0.3}$ for cluster at redshift $z = 0.33$ relative to the one at $z = 0.035$, in consistent with the result ($1.4^{+0.4}_{-0.3}$) of Henry et al. (1994). Though the cluster temperature evolution since intermediate redshift is moderate, it may account for the mass discrepancy we report in the present paper.

We now discuss briefly the significance of the consistency/discrepancy between the cluster masses derived from gravitational lensing, dynamical analysis and X-ray observations.

Both gravitational lensing and “virial” methods yield nearly the same cluster masses, which have several implications: First, galaxy velocity dispersion indeed provides a good estimate of cluster mass. Second, the dark matter particles and the galaxies have approximately the same velocity dispersion, i.e., there is no velocity bias in clusters of galaxies. Third, mass follows the light. These arguments are comparable with the recent dynamical analysis of the CNOC cluster sample (Carlberg et al. 1996), which has found strong evidence that galaxies are effectively in equilibrium with their host cluster. However, our finding disagrees with the numerical result that the velocity biasing parameter is $\sim 0.7\text{--}0.8$ (Carlberg & Dubinski 1991; Couchman & Carlberg 1992).

On the other hands, cluster mass estimate based on the X-ray temperature assuming an isothermal hydrostatic equilibrium has systematically underestimated cluster masses

by a factor of $\sim 2-3$ as compared with gravitational lensing and “virial” method, which demonstrates that the gas particles may not be a good tracer of the gravitational potential of the cluster. The recent high-spectral resolution observations do reveal the occurrence of complex temperature maps, indicating the on-going merger activities in clusters and the cluster evolution with cosmic epoch. Overall, the simplification of modeling the temperature (isothermal) and gas density profile (spherical) is responsible for the deficit of the X-ray cluster mass detected in this paper. One may also attribute the mass discrepancy to the nonthermal pressure in clusters (Loeb & Mao 1994; Ensslin et al. 1997), which affects the gas particles while produces no effect on galaxy distribution and velocity dispersion. Finally, it is pointed out that our results still contain large scatters due to the scarcity of the lensing data, and a large cluster sample will be needed to confirm our finding.

Useful discussion with François Hammer and Shude Mao and valuable suggestions by an anonymous referee are gratefully acknowledged. WXP wishes to thank the hospitality of DAEC, Observatoire de Paris-Meudon, where part of this research was made. This work was supported by the National Science Foundation of China.

Table 1: Lensing cluster sample

REFERENCES

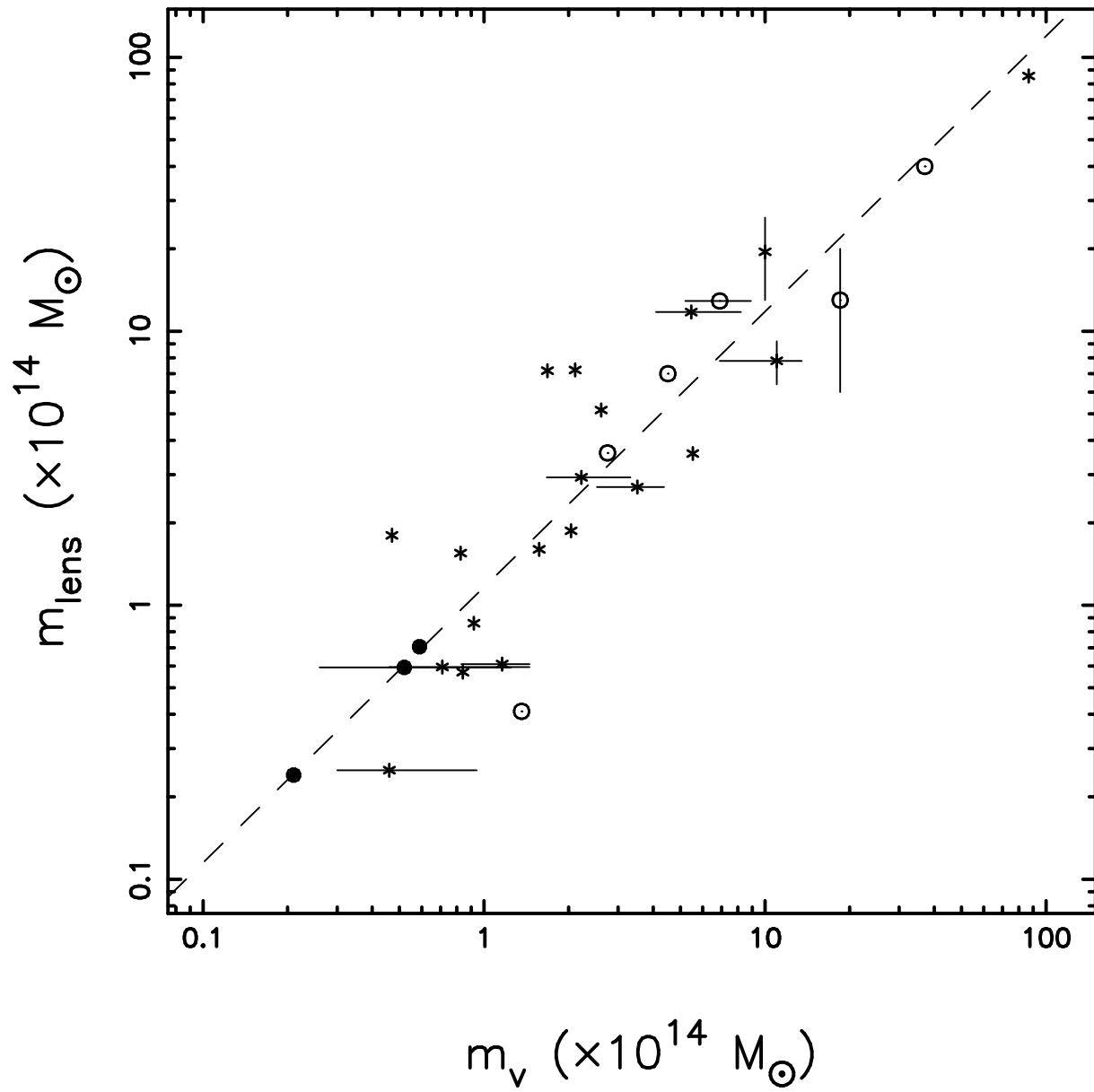
- Allen, S. W., Fabian, A. C., & Kneib, J. P., 1996, 279, 615
- Bahcall, N. A., & Lubin, L. M. 1994, ApJ, 426, 513
- Bartelmann, M., & Steinmetz, M. 1996, MNRAS, 283, 431
- Bonnet, H., Mellier, Y., & Fort, B. 1994, ApJ, 427, L83
- Carlberg, R. G., & Dubinski, J. 1991, ApJ, 369, 13
- Carlberg, R. G., et al. 1996, astro-ph/9611204
- Cen, R. 1996, ApJ, submitted; astro-ph/960800
- Couchman, H. M. P., & Carlberg, R. G. 1992, ApJ, 389, 453
- Edge, A. C., et al. 1994, A&A, 289, L34
- Edge, A. C., & Stewart, G. C. 1991, MNRAS, 252, 414
- Edge, A. C., Stewart, G. C., Fabian, A. C., & Arnaud, K. A. 1990, MNRAS, 245, 559
- Ensslin, T. A., Biermann, P. L., Kronberg, P. P., & Wu, X. P. 1997, ApJ, in press
- Fabian, A. C., Crawford, C. S., Edge, A. C., & Mushotzky, R. F. 1994, MNRAS, 267, 779
- Fahlman, G., Kaiser, N., Squires, G., & Woods, D. 1994, ApJ, 437, 56
- Fort, B., & Mellier, Y. 1994, A&A Rev., 5, 239
- Gioia, M., et al. 1990, ApJ, 356, L35
- Gioia, M., et al. 1995, A&A, 297, L75
- Girardi, M., Fadda, D., Giuricin, G, Mardirossian, F., & Mezzetti, M. 1996, ApJ, 457, 61
- Giraud, E. 1988, ApJ, 334, L69
- Grossman, S. A., & Saha, P. 1994, ApJ, 431, 74
- Hammer, F. 1991, ApJ, 383, 66

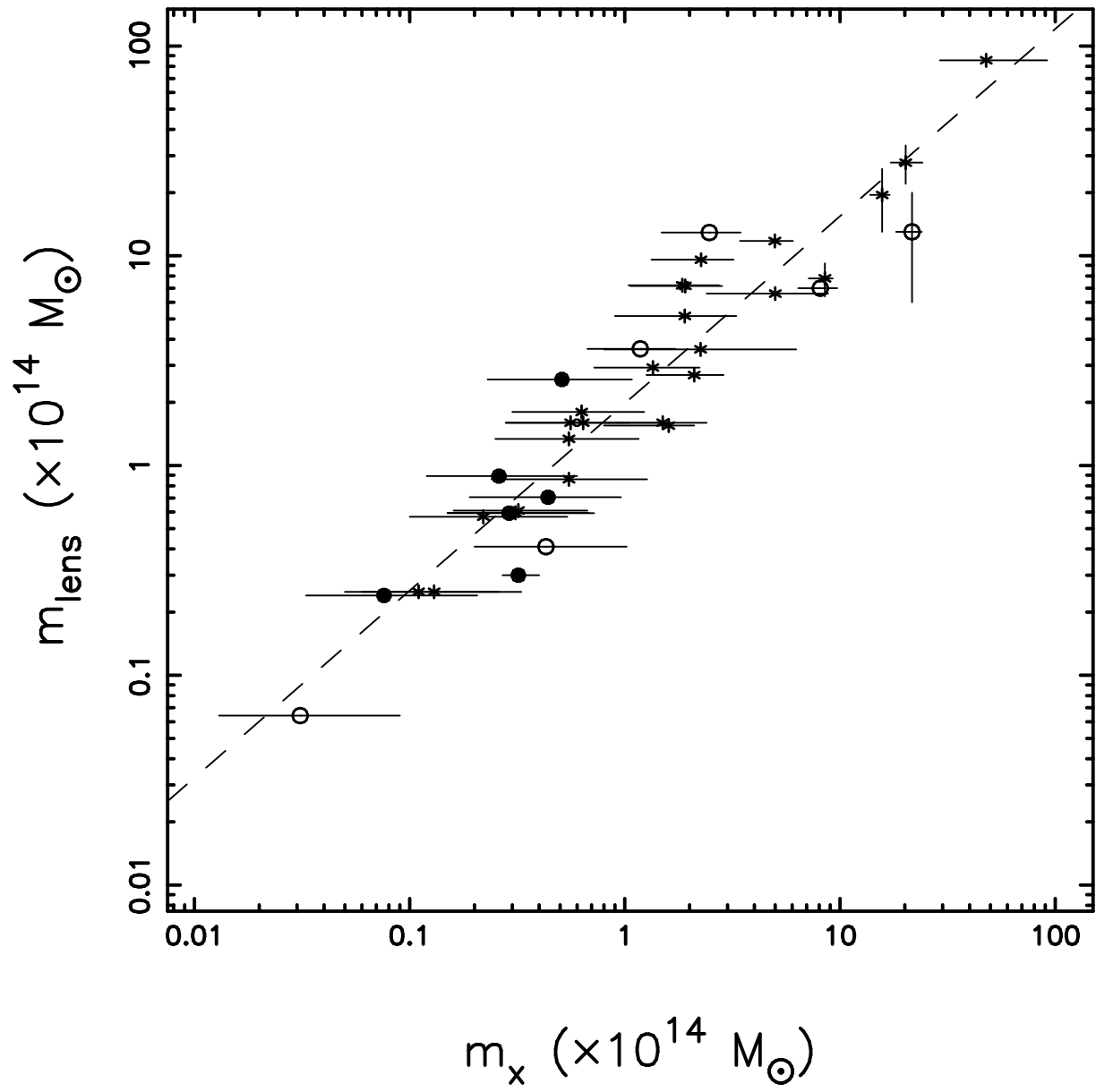
- Hammer, F., Le Fèvre, O., Jones, J., Rigaut, F., & Soucail, G. 1989, *A&A*, 208, L7
- Henriksen, M. J., & Markevitch, M. L. 1996, *ApJ*, 466, L79
- Henriksen, M. J., & White III, R. E. 1996, *ApJ*, 465, 515
- Henry, J. P., et al. 1992, *ApJ*, 386, 406
- Henry, J. P., Jiao, L., Gioia, I. M. 1994, *ApJ*, 432, 49
- Jones, C., & Forman, W. 1984, *ApJ*, 276, 38
- Kneib, J. P., et al. 1996, *A&A*, in press
- Kneib, J. P., Mellier, Y., Fort, B., & Mathez, G. 1993, *A&A*, 273, 367
- Lavery, R. J., & Henry, J. P. 1988, 329, L21
- Le Fèvre, O., Hammer, F., Angonin, M. C., Gioia, I. M., & Luppino, G. A. 1994, *ApJ*, 422, L5
- Loeb, A., & Mao, S. 1994, *ApJ*, 435, L109
- Lubin, L. M., & Bahcall, N. A. 1993, 415, L17
- Luppino, G. A., & Gioia, I. M. 1992, *A&A*, 265, L9
- Luppino, G. A., Gioia, I. M., Annis, J., Le Fèvre, O., & Hammer, F. 1993, *ApJ*, 416, 444
- Luppino, G. A., & Kaiser, N. 1996, *ApJ*, submitted; astro-ph/9601194
- Markevitch, M. 1996, *ApJ*, 465, L1
- Mathez, G., Fort, B., Mellier, Y., Picat, J.-P., & Soucail, G. 1992, *A&A*, 256, 343
- Mellier, Y., Fort, B., & Kneib, J. P. 1993, *ApJ*, 407, 33
- Mewe, Q., Lemen, J. R., & van den Oord. G. H. J. 1986, *A&AS*, 65, 511
- Miralda-Escudé, J., & Babul, A. 1995, *ApJ*, 449, 18
- Pelló, R., et al. 1991, *ApJ*, 366, 405

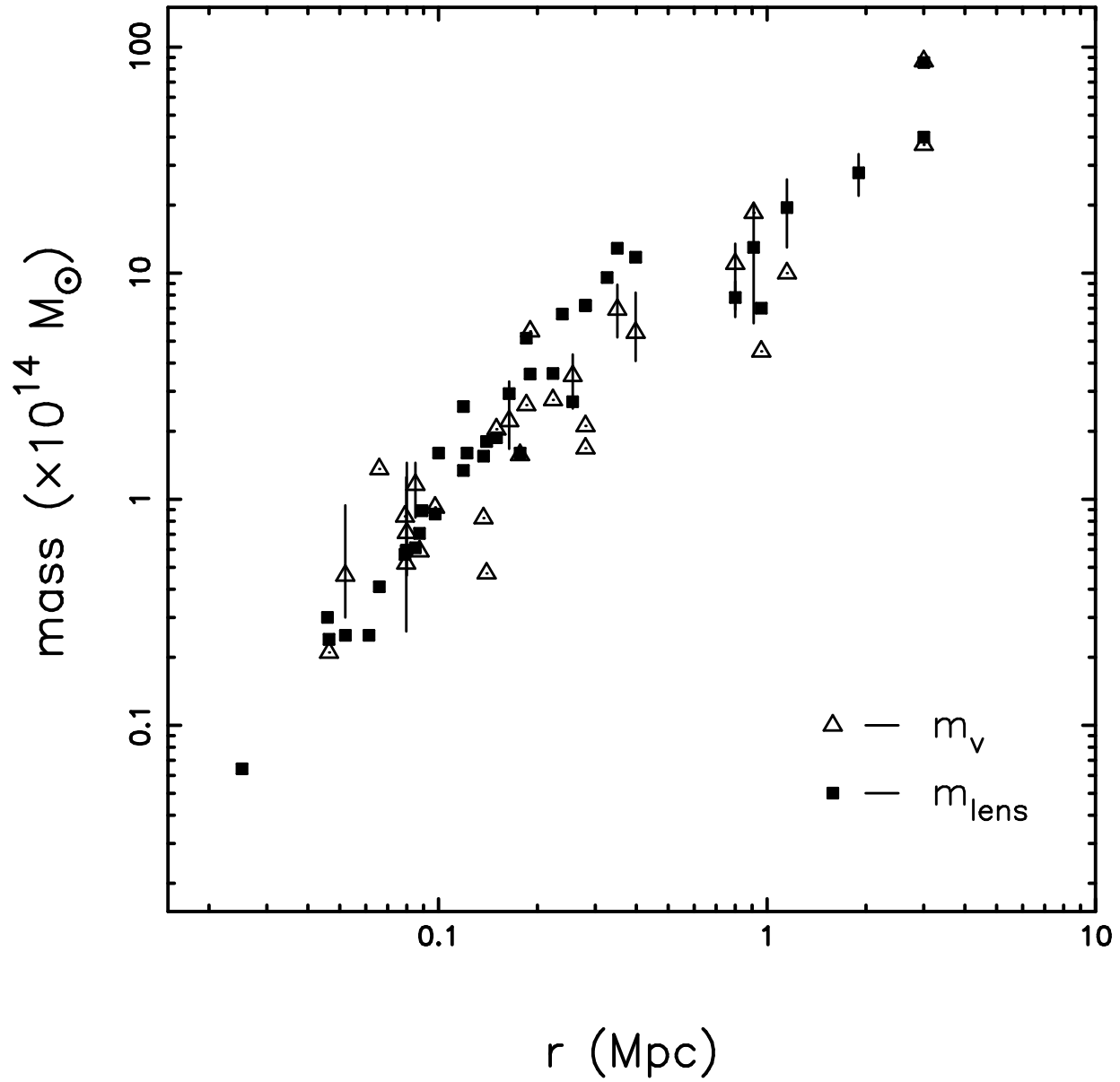
- Pierre, M., Soucail, G., Höhringer, H., & Sauvageot, J. L. 1994, 289, L37
- Schindler, S. et al. 1995, A&A, 299, L9
- Smail, I., Couch, W. J., Ellis, R. S., & Sharples, R. M. ApJ, 1995a, 440, 501
- Smail, I., et al. 1995b, MNRAS, 277, 1
- Smail, I., et al. 1997, ApJ, in press
- Squires, G., et al. 1996a, ApJ, submitted; astro-ph/9603050
- Squires, G., Kaiser, N., Fahlman, G., Babul, A., & Woods, D. 1996b, ApJ, 469, 73
- Tyson, J. A., & Fischer, P. 1995, ApJ, 446, L55
- Van Waerbeke, L., & Mellier, Y. 1996, in the Proc. of the XXXIst Recontres de Moriond,
in press.
- Wallington, S., & Kochanek, C. S. 1995, ApJ, 441, 58
- Wu, X. P. 1994, ApJ, 436, L115
- Wu, X. P. 1996, Fund. Cosmic Phys., 17, 1
- Wu, X. P., & Fang, L. Z. 1996, ApJ, 467, L45 (Paper I)
- Wu, X. P., & Hammer, F. 1993, MNRAS, 262, 187

Fig. 1.— Gravitational lensing derived cluster mass m_{lens} plotted against dynamical cluster mass m_v (a) and X-ray cluster mass m_x (b). Additionally, cluster morphologies are represented by different symbols: open circles – regular, filled circles – elliptical and asterisks – irregular. The dashed lines are the least square fits of the data to a power-law.

Fig. 2.— Comparisons of cluster radial mass distributions derived from gravitational lensing and dynamical method (a) and from gravitational lensing and X-ray gas hydrostatic equilibrium (b). Note that the β parameter is taken to be $\beta_{fit} = 0.67$ in (b).







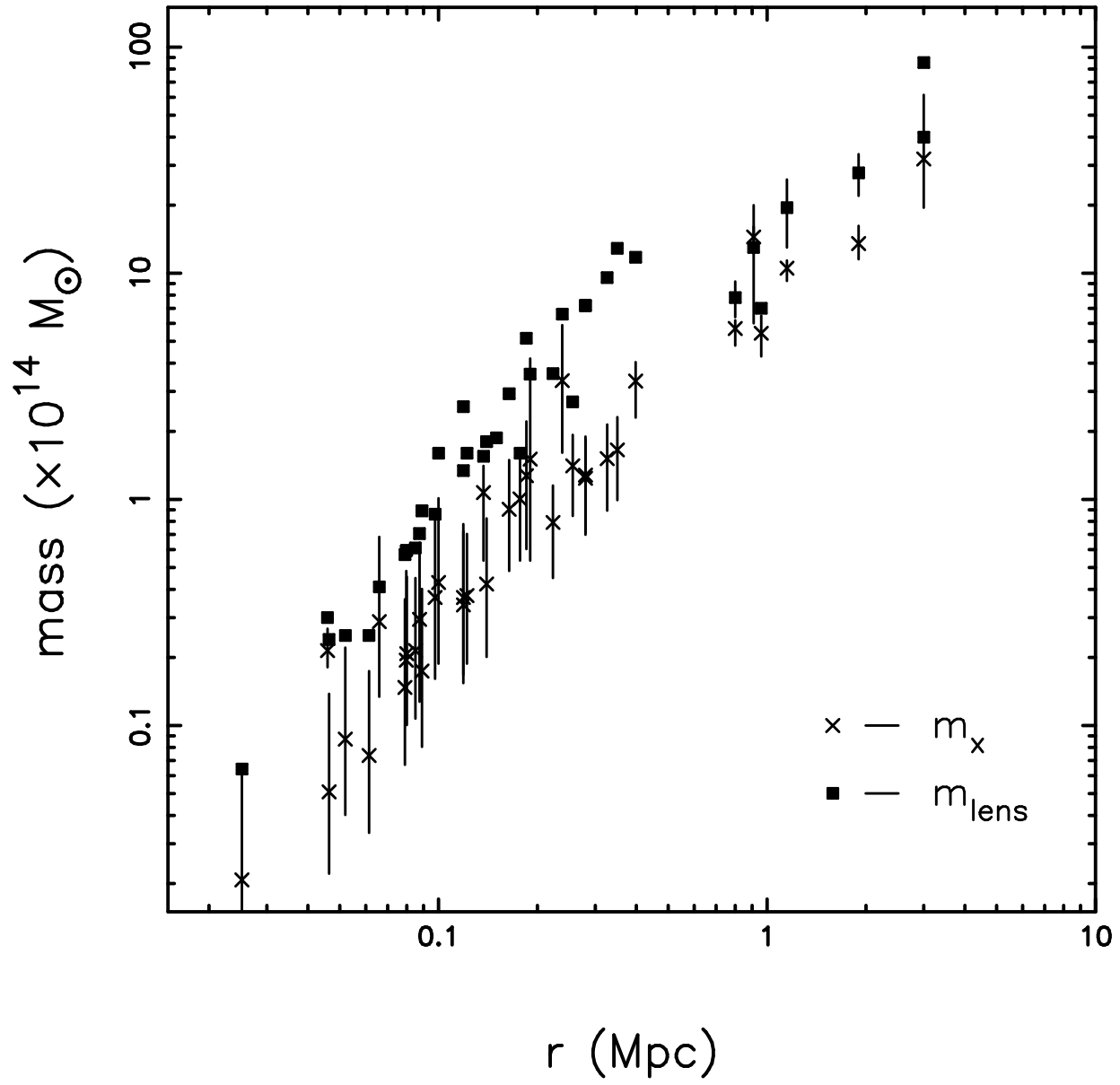


Table 1: Lensing cluster sample

cluster	z_d	L_x (ϵ) ^a	T ^b	σ	mor. ^c	m_x ^d	m_v ^d	arc/w.l. ^e	z_s	r (Mpc) ^f	m_{lens} ^d	ref. ^g
A370	0.374	14.5 _(0.7-6)	8.6 ^{+0.5} _{-0.4}	1367 ⁺³¹⁰ ₋₁₈₄	I	1.4 ^{+0.9} _{-0.6}	2.2 ^{+1.1} _{-0.6}	arc	0.725	0.16	2.9	1
						5.0 ^{+1.1} _{-1.6}	5.5 ^{+2.8} _{-1.4}	arc	1.3(?)	0.40	12	1
A963	0.206	9.49 ₍₂₋₁₀₎	7.3 ^{+0.5} _{-0.4}	1100 ⁺⁴⁸⁰ ₋₂₁₀	I	0.13 ^{+0.20} _{-0.07}	0.46 ^{+0.48} _{-0.16}	arc	0.771	0.052	0.25	2
						0.31 ^{+0.37} _{-0.16}	0.71 ^{+0.74} _{-0.25}	arc		0.080	0.60	2
A1689	0.17	26.8 ₍₂₋₁₀₎	10.5 ^{+0.7} _{-0.7}	1989	I	2.3 ^{+4.0} _{-1.5}	5.5	arc		0.19	3.6	3
						48 ⁺⁴⁴ ₋₁₉	87	w.l.		3.	89	3
A1104	0.155	8.0 _(0.1-2.4)	6.9 ^{+1.4} _{-1.0}		E/I	0.031 ^{+0.059} _{-0.018}		arc		0.025	0.064	4
A2163	0.201	70 ₍₂₋₁₀₎	14.7 ^{+1.1} _{-1.0}	1680	E(?)	0.43 ^{+0.59} _{-0.23}	1.36	arc	0.728	0.066	0.41	5
					E(?)	21.6 ^{+2.4} _{-3.4}	18.5	w.l.		0.90	13 ⁺⁷ ₋₇	6
A2218	0.175	6.5 _(0.5-4.5)	6.6 ^{+0.3} _{-0.3}	1370 ⁺¹⁶⁰ ₋₂₁₀	I	0.32 ^{+0.35} _{-0.16}	1.2 ^{+0.3} _{-0.3}	arc	0.702	0.085	0.61	7
						8.5 ^{+0.8} _{-1.4}	11.0 ^{+2.5} _{-4.1}	w.l.		0.8	7.8 ^{+1.4} _{-1.4}	7
						2.1 ^{+0.8} _{-0.8}	3.5 ^{+0.9} _{-1.0}	arc	1.034	0.26	2.7	7
A2219	0.225	18 _(0.1-2.4)	9.9 ^{+2.2} _{-1.6}		I	0.64 ^{+0.87} _{-0.36}		arc		0.10	1.6	8
A2280	0.326	5.06 _(0.5-2)	6.9 ^{+1.3} _{-1.0}	948 ⁺⁵¹⁶ ₋₂₈₅	R/E	0.29 ^{+0.43} _{-0.14}	0.52 ^{+0.73} _{-0.26}	arc		0.080	0.59	9
A2390	0.231	4.67 _(0.7-3.5)	8.5 ^{+0.5} _{-0.5}	1093	I	1.5 ^{+0.9} _{-0.7}	1.57	arc	0.913	0.18	1.6	10
						15.7 ^{+1.3} _{-1.9}	10.0	w.l.		1.15	19.5 ^{+6.5} _{-6.5}	11
S295	0.299	2.0 _(bol.)	6.7 ^{+7.8} _{-1.5}	907	I	1.6 ^{+0.5} _{-0.8}	0.825	arc	0.93	0.14	1.6	12
U0500	0.316	(1.) _(0.1-2.4)	(2.8 ^{+0.2} _{-0.1})	1375	I	(0.38 ⁺²⁸ _{-0.18})	2.0	arc	0.913	0.15	1.9	13
U0024	0.391	2.7 ₍₂₋₁₀₎	4.7 ^{+0.3} _{-0.2}	1300	E	1.2 ^{+0.5} _{-0.5}	2.8	arc	1.39(?)	0.22	3.6	14
							37	w.l.		3.0	40	15
U0302	0.423	4.8 _(0.7-5)	6.0 ^{+0.3} _{-0.3}		I	0.56 ^{+0.49} _{-0.28}		arc		0.12	1.6	16
U2244	0.328	1.5 _(0.5-4.5)	4.4 ^{+0.2} _{-0.2}		I	0.11 ^{+0.15} _{-0.06}		arc	2.237	0.061	0.25	17
MS0440	0.190	4.01 _(0.3-3.5)	4.9 ^{+0.8} _{-0.6}		R	0.26 ^{+0.34} _{-0.14}		arc	0.53	0.089	0.89	18
MS0451	0.55	20 _(0.3-3.5)	9.7 ^{+2.0} _{-1.5}	1371	I	1.9 ^{+1.4} _{-1.0}	2.61	arc		0.19	5.2	19
MS1006	0.221	4.82 _(0.3-3.5)	5.3 ^{+0.9} _{-0.7}	906	I	0.22 ^{+0.32} _{-0.12}	0.47	arc		0.079	0.57	19
						0.63 ^{+0.60} _{-0.33}	0.84	arc		0.14	1.8	19
						1.9 ^{+0.9} _{-0.9}	1.68	arc		0.28	7.2	19
MS1008	0.301	4.49 _(0.3-3.5)	5.1 ^{+0.9} _{-0.7}	1054	I	1.7 ^{+0.9} _{-0.8}	2.11	arc		0.26	6.1	19
MS1054	0.826	9.02 _(0.3-3.5)	6.9 ^{+1.3} _{-1.0}		I	20.2 ^{+4.0} _{-3.4}		w.l.		1.9	28 ⁺⁶ ₋₆	20
MS1224	0.327	4.61 _(0.3-3.5)	5.2 ^{+0.9} _{-0.7}	802	E/I	8.1 ^{+1.6} _{-1.7}	4.5	w.l.		0.96	7.0	21
MS1445	0.259	16.0 _(0.3-3.5)	8.8 ^{+1.8} _{-1.4}	1133	I	0.55 ^{+0.72} _{-0.31}	0.92	arc		0.098	0.86	19
MS1621	0.426	4.55 _(0.3-3.5)	5.1 ^{+0.9} _{-0.7}	793	R	0.076 ^{+0.13} _{-0.043}	0.21	arc		0.046	0.24	22
MS1910	0.246	4.38 _(0.3-3.5)	5.0 ^{+0.9} _{-0.7}		I	2.3 ^{+0.9} _{-0.9}		arc		0.33	9.6	19
MS2053	0.583	5.8 _(0.3-3.5)	5.7 ^{+1.0} _{-0.8}		R	0.51 ^{+0.57} _{-0.28}		arc		0.119	2.6	22
MS2137	0.313	15.6 _(0.3-3.5)	8.7 ^{+1.7} _{-1.3}	960	R/E	0.44 ^{+0.52} _{-0.25}	0.59	arc		0.088	0.71	23
MS2318	0.187	6.84 _(0.3-3.5)	6.1 ^{+1.1} _{-0.9}		I	0.55 ^{+0.61} _{-0.30}		arc		0.12	1.3	19
AC114	0.31	4.0 _(0.1-2.4)	5.0 ^{+0.9} _{-0.7}	1649 ⁺²²⁰ ₋₂₂₀	I(?)	2.5 ^{+1.0} _{-1.0}	6.9 ^{+2.0} _{-1.7}	arc	0.639	0.35	13	24
PKS0745	0.103	28 ₍₂₋₁₀₎	10.6 ^{+0.7} _{-0.7}		R	0.32 ^{+0.08} _{-0.05}		arc	0.433	0.046	0.30	25
RXJ1347	0.451	62 _(0.1-2.4)	17.5 ^{+5.4} _{-3.9}		I	5.0 ^{+3.8} _{-2.6}		arc		0.24	6.6	26

Accepted for publication in MNRAS on 25 Jan 1997

^aX-ray luminosity in unit of 10^{44} erg s⁻¹ measured in the ϵ energy band (keV).

^bEstimated temperature (keV) from the L_x - T relation.

^cCluster X-ray/optical morphology: E-elliptical, I-irregular and R-regular.

^dProjected cluster mass within radius r in unit of $10^{14}M_{\odot}$.

^eLensing phenomenon: arc(s) or weak lensing (w.l.).

^fDistance from the center of cluster where arc(s) and/or weak lensing are detected.

^gOnly one reference is provided for lensing features.

References – (1)Kneib et al. 1993; (2)Lavery & Henry 1988; (3)Tyson & Fischer 1995; (4)Pierre et al. 1994; (5)Miralda-Escudé & Babul 1995; (6)Squires et al. 1996a; (7)Kneib et al. 1996; (8)Smail et al. 1995b; (9)Gioia et al. 1995; (10)Pelló et al. 1991; (11)Squires et al. 1996b; (12)Edge et al. 1994; (13)Giraud 1988; (14)Wallington & Kochanek 1995; (15)Bonnet et al. 1994; (16)Mathez et al. 1992; (17)Hammer et al. 1989; (18)Luppino et al. 1993; (19)Le Fèvre et al. 1994; (20)Luppino & Kaiser 1996; (21)Fahlman et al. 1994; (22)Luppino & Gioia 1992; (23)Mellier et al. 1993; (24)Smail et al. 1995a; (25)Allen et al. 1996; (26)Schindler et al. 1995.